Brazilian Journal of Analytical Chemistry
2025, Volume 12, Issue 48, pp 248-266
doi: 10.30744/brjac.2179-3425.AR-162-2024

ARTICLE

Integrating an Extended-Gate Field Effect Transistor in Microfluidic Chips for Chloride and Thiocyanate Potentiometric Detection

Dhaniella Cristhina de Brito Oliveira*[1], Fernando Henrique Marques Costa[1], Renato Massaroto Beraldo[2], José Alberto Fracassi da Silva[1]

[1]*Instituto de Química, Universidade Estadual de Campinas Rua Monteiro Lobato, 270, Cidade Universitária, 13083-862, Campinas, SP, Brazil*

[2]*Faculdade de Engenharia Elétrica e de Computação, Universidade Estadual de Campinas, Avenida Albert Einstein, 400, Cidade Universitária, 13083-852, Campinas, SP, Brazil*

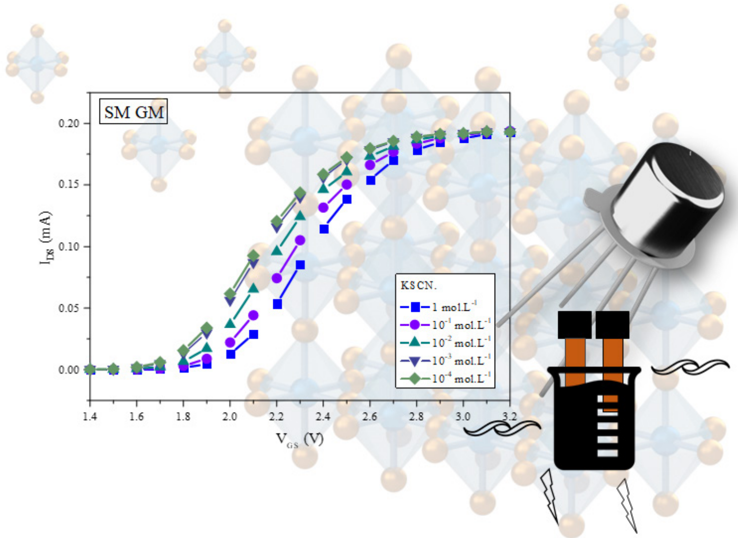

In the last five years, the development of sensors based on Extended Gate Field Effect Transistors has grown by at least 223%. In this article we discuss the concepts involved behind the potentiometric response resulting from the use of EGFETs in recognizing chloride and thiocyanate ions. The results are discussed considering two ways of obtaining the response: current modulation between source-drain and the variation in threshold voltage caused by the different concentrations of the solutions. The current sensitivity for chloride was 0.0330 mA$^{0.5}$ mol^{-1} L and 0.1762 mA$^{0.5}$ mol^{-1} L for thiocyanate, the linear response ranged from 1.0 to 1.0x10^{-5} mol L^{-1} for both static and dynamic setups with R^{2} of 0.9952 and 0.9992. The voltage sensitivity was 47.4 mV dec^{-1} and 52.96 mV dec^{-1} with R^{2} of 0.9999 for chloride. For the thiocyanate detection, the linear range from 1.0 to 1.0x10^{-5} mol L^{-1} with 58.88 mV dec^{-1} and 137.06 mV dec^{-1} to voltage sensitivity, with R^{2} of 0.9862. The voltage sensitivity obtained with the plug injection system was 170.78 mV dec^{-1} ranging from 1.0 mol L^{-1} to 1.0x10^{-4} mol L^{-1}, with a R^{2} of 0.9436. From our knowledge, this is the first demonstration of integration of EGFETs to a 3D-printed microfluidic device in recognizing chloride and thiocyanate ions.

Keywords: chloride detection, EGFET, thiocyanate, potentiometry, microfluidic device, 3D printing

Cite: Oliveira, D. C. B.; Costa, F. H. M.; Beraldo, R. M.; Silva, J. A. F. Integrating an Extended-Gate Field Effect Transistor in Microfluidic Chips for Chloride and Thiocyanate Potentiometric Detection. *Braz. J. Anal. Chem.* 2025, *12* (48), pp 248-266. http://dx.doi.org/10.30744/brjac.2179-3425.AR-162-2024

Submitted October 29, 2024, Resubmitted February 3, 2025, Resubmitted 2nd time March 3, 2025, Accepted April 24, 2025, Available online May 12, 2025.

This article was submitted to the BrJAC special issue celebrating the achievement of Journal Impact Factor.

INTRODUCTION

Sensors that use field effect transistors with the extended gate (EGFETs) have gained special attention in the manufacture of detection systems. They are easy to handle and can be used for a wide range of applications due to the easiness of coupling sensitive membranes and their high sensitivity.[1-3] According to a survey in the Science Direct platform, the number of publications related to EGFETs has grown by at least 223% in the last five years.

Field-effect transistors (FET) based sensors, such as EGFETs, work by modulating the number of charge carriers in a channel formed in a semiconductor material by means of an external electric field.[4-6] A metal-oxide-semiconductor (MOS) FET is made by depositing layers of an insulator oxide and a conductive material, to make the electrical contacts, over an intrinsic semiconductor.[7] In this way, three interfaces are formed, namely metal-oxide, oxide-semiconductor and semiconductor-metal. The structure of a FET consists of terminals called substrate, source, drain and gate.[7]

In an EGFET, the gate terminal is extended to the testing solution by attaching an electrode modified with a material sensitive to a chemical species. The electrical potential developed at the electrode is transferred to the gate terminal that modulated the conductive of the channel formed between the source and drain, at the oxide-semiconductor interface. The indicator electrode is electrically charged by the accumulation of species on its surface, which induces a flow of opposing charges at the oxide-semiconductor interface, between the source and the drain.[4,5,7-9] The insulating oxide mediates the charges that are polarized during the operation of the device, causing the current between the drain and source terminals to be controlled by the variation in the electrical potential onto the gate terminal, characterizing the field effect.[10-13]

So, in FET sensors one obtains a typically potentiometric response, and the current between indicator and reference electrode is negligible.[7] One fact that draws attention to the use of potentiometric methods is that they can be used in the most varied types of ionic detection and, as a result, they have a wide laboratory scope. One inherent disadvantage of potentiometry is its low sensitivity compared to other electrochemical techniques. Also, depending on the selectivity of the sensing membrane, the sensor can be responsible to other species in the sample, demanding, for example, an additional separation step to remove interfering ions.[14,15] The use of FETs for potentiometric sensors is useful for expanding the sensitivity range of sensors since they are able to work with small input signals due to their signal amplifying function. Potentiometric configurations using EGFETs integrated into microfluidic chips have been reported in the literature and allow for low consumption of reagents and samples, with a simplified recognition process and the possibility of automation for application in remote locations.[16,17] In this study, we used the operating principle of EGFETs to develop a sensor for measuring the concentration of chloride and thiocyanate in various media, as a proof-of-concept research. In addition, we have manufactured a bench measurement system in order to reduce the costs of using equipment such as semiconductor parameter analyzers, and to contribute to the technology of use of EGFETs in point-of-care devices.

As far as we know, EGFETs have not yet been tested in chloride and thiocyanate detection systems. Mostly, they have been applied to detecting the hydrogen potential (pH) of different samples with the manufacture of new H^+ proton recognition membranes.[18-27]

Abnormal levels of chloride are responsible for causing damage to the skin, respiratory and nervous systems, as well as the occurrence of other diseases, since this halide acts in the body's functional activities, maintaining the electrochemical neutrality of extracellular fluids.[28] Research has shown that high chloride levels are also responsible for diseases such as cystic fibrosis and renal tubular disorders,[29,30] among others. In water, chloride excess is also responsible for altering test performance in the laboratory, such as in catalysis, capacitance measurement techniques and spectroscopy.[31] Therefore, chloride ion measurements are extremely important in various areas of economic, social and environmental development.

The thiocyanate ion (SCN^-) is a pseudo-halide formed mainly by the reaction between cyanide and thiosulphate.[32,33] It is used in agricultural, food and industrial procedures.[34,35] Waste containing this species when disposed of near rivers and lakes can alter the aqueous pH and the concentration of cyanides in the water due to radiation and chlorination. Released into the atmosphere through car exhaust or as a by-product of cigarette smoke, thiocyanate can cause serious environmental problems and pose risks to human health.[36,37] In the human body, excess of SCN^- can inhibit the use of iodine by the endocrine gland, causing alterations in thyroid hormones and triggering or fueling problems such as thyroid disease.[38,39] Once iodine transport is altered in the glands, there can be an increase in the size of the thyroid causing goiters, there can also be neurological consequences in developing fetuses, an increased risk of triggering cancers, cardiovascular problems, altered protein dialysis, respiratory and inflammatory diseases, psychotic symptoms, abdominal pain, kidney problems, hyperreflexia, muscle weakness, delirium, convulsions, among other factors that can lead to coma and death.[36,38-43]

In this research, we built electrochemical cell systems using commercial MOSFETs, as many studies in the literature have done,[44-48] and we discuss the concepts involved behind the potentiometric response resulting from the use of EGFETs in recognizing chloride and thiocyanate ions using simple metallic indicator electrode, without making new recognition membranes.

MATERIALS AND METHODS

Reagents

All reagents were of analytical grade and were used as received, except when otherwise indicated. Potassium chloride (KCl), Sodium nitrate ($NaNO_3$), Sodium chloride (NaCl) were purchased from Synth (Diadema, SP, Brazil) and Potassium thiocyanate (KSCN) from Sigma-Aldrich (Darmstadt, Germany). Clear acrylic resin of curing wavelength 405 nm was purchased from Anycubic (Anycubic, Hong Kong, China) and synthetic urine, saliva, and sweat were purchased from BioChemazone (Leduc, AB, Canada). The solutions were prepared in deionized water (DI) with resistivity of 18.2 MΩ cm at 25 ºC, in 0.5 mol L^{-1} $NaNO_3$, and in synthetic urine, saliva, and sweat.

3D-printed device

Microfluidic devices were prepared using a Phrozen Sonic Mini 8K 3D printer (Phrozen Technology, Taiwan, China). The software used to create the 3D object was Fusion 360 Autodesk (San Rafael, CA, USA). The software used to slice the object was Chitubox version 1.8. The device was a single-channel structure with inlet and outlet reservoirs, as shown in Figure 1, which allowed for efficient tubing connection.

The microchip device of Figure 1 was 60 mm long, 20 mm wide and 2.1 mm thick. There was only one flow channel projected onto the chip, designed as 0.200 mm deep and 0.100 mm wide. There were circular reservoirs at each end of the channel with a diameter of 3 mm and a depth of 0.200 mm. Along the fluid channel there were two holes with 1.20 mm in diameter and 0.200 mm in depth, used as ports for the working and reference electrodes, 7.88 mm apart. The channel was sealed by a 0.100 mm thick layer.

Once printed, the device was finalized by connecting 4 mm diameter, 170 mm long Tygon® tubes. A 0.60 mm diameter needle was used to attach the Tygon® tube to a syringe pump. Finally, the reference and indicator electrodes were carefully attached to the device and glued with the same photocurable resin used in the 3D printing. The reference electrode was a lab-made Ag/AgCl electrode in 3.0 mol L^{-1} KCl solution. The indicator electrode was a 100 mm x 0.100 mm rectangular piece of silver sheet where an AgCl film was electrochemically deposited. The reference electrode was characterized by cyclic voltammetry and potentiometric response over different time spans. The characterization results were compared to those of a commercial reference electrode.

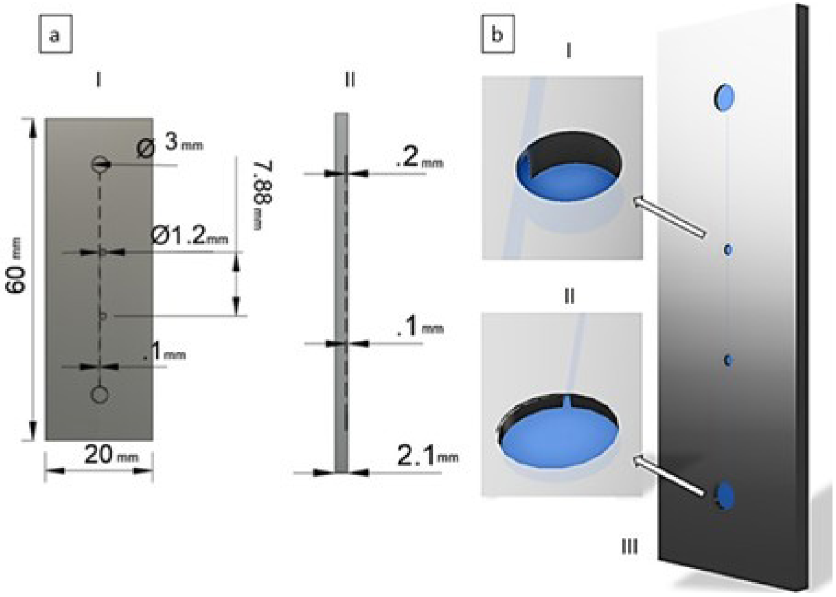

Figure 1. Microfluidic device manufactured by digital light processing. (a) CAD drawing of the device using Fusion 360, showing the projected dimensions of the reservoirs, flow channels, electrode port, width and length of the device in the front (I) and side (II) views. (b) Rendered draw of the device, highlighting the design of the (I) electrode port, (II) the outlet reservoir, and (III) a whole view of the microfluidic device.

EGFET and measurements

A commercial MOSFET model 2N4351 (Motorola, Chicago, IL, USA) NMOS was used in this research. 8.2 KΩ resistors were also obtained commercially. Equipment such as voltage sources (Minipa MPL 3303M, Shanghai, China), a syringe pump (Harvard Apparatus, Holliston, MA, USA), an Analogue - Digital Interface Module (National Instruments NI USB 6341, Budapest, Hungary), a Semiconductor Characterizing System (KI 4200 MPSMU, Keithley, Cleveland, OH,USA), a modulator, a metal box, copper/phenolite board, copper wire and electrical interconnectors were also used to carry out the measurements. The instrumental setups used in this research can be viewed in Figure 2.

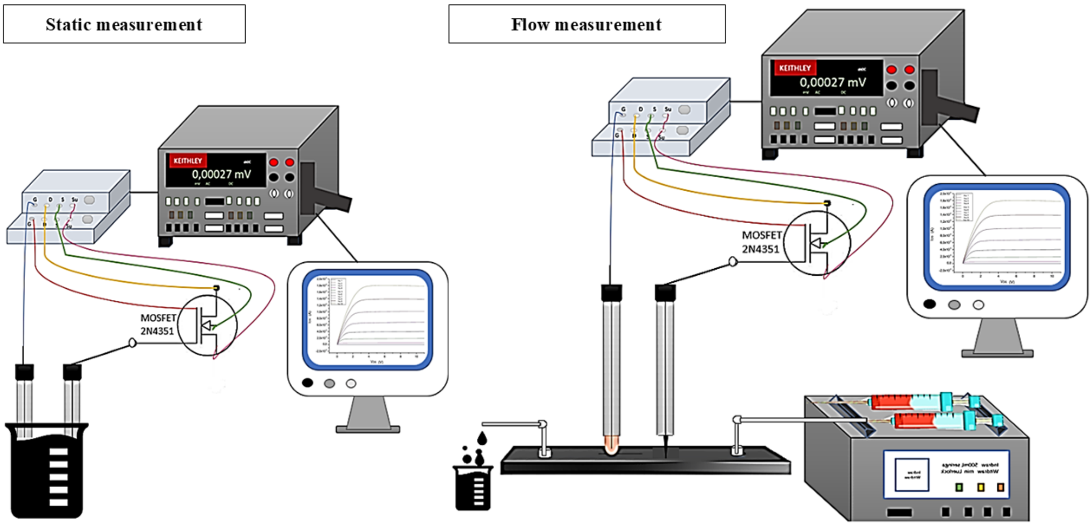

Figure 2. Static measurement and flow measurement setups.

The static measurement system of Figure 2 consisted of a reference and indicator electrodes immersed in a 10 mL beaker containing the analyte solution. For the flow measurements of Figure 2, the reference and indicator electrodes were positioned in pre-designed holes in the microfluidic chip, as described in Figure 1. A syringe pump was used to control the flow in the microfluidic channel. In both systems of Figure 2, the reference electrode was connected directly to a source-measure unit (SMU) to receive the signals from the Parameter Analyzer (KI 4200 MPSMU, Keithley). The indicator electrode was connected to the gate terminal of the Motorola model 2N4351 commercial NMOS MOSFET and also connected to the electrical unit for contact with the Keithley. A computer integrated into the Keithley allowed access and storage of the data generated during the measurements.

With the systems in Figure 2, curves of drain-source current (I_{DS}) versus drain-source voltage (V_{DS}) as a function of sample concentration and gate-source voltage (V_{GS}) were obtained. First, we used the data to extract the slopes and the error to check the best operating region for the system. Next, two different types of electrical measurements were made, under three different conditions for each sample: (1) measurement with fixed V_{GS} and V_{DS} and measurement of the threshold voltage (V_T) with the indicator and reference electrodes immersed in a beaker containing 5 mL of sample solution. The data from this measurement is referred throughout the text as static measurements (SM). The V_{GS} quoted in the measurements with fixed V_{DS} refers to the potential applied to the reference electrode in relation to the ground (0 V); (2) the same procedure as for measurement 1 with the electrodes in the channel of the fabricated microchip at a constant flow of 500 µL min^{-1} by using a syringe pump. These measurements are referred to flow measurements (FM); (3) the same procedure as for measurement 2 but with the syringe pump uninterruptedly injecting the blank solution (electrolyte in which the solutions were prepared) while the different concentrations of the analyte (1.0 mol L^{-1} to 1.0x10^{-6} mol L^{-1}) were plug injected every minute. Throughout the text, we refer to these measurements as plug injection (PIn). For the last measurement test we used a lab-made setup developed for this purpose.

RESULTS AND DISCUSSION

In the instrumentation for EGFETs, the control electrode, commonly known as the reference electrode, does not act exactly as a reference electrode as we know it in electrochemical methods.[49] A voltage is applied to it, which is communicated capacitively via interfacial electrical double layers to the indicator electrode connected to the gate of the commercial MOSFET, causing the device to have enough charge to leave the inertial state. Another power supply is responsible for applying a voltage to the drain/source. In this configuration, the drain to source current (I_{DS}) can be modulated by the gate-to-source voltage (V_{GS}). Since the gate is opened and in contact with the sample solution, its potential is intimately related to the interaction with ion species at the electrode surface.[49]

A FET has three operating regions: cut-off, triode and saturation. The cut-off region corresponds to the moment when there is no induced channel and the voltage between the gate and source is lower than the voltage required for the device to operate, which is why the device is switched off ($V_{GS} \leq V_T$). To reach the operating region, the sensor must have a voltage above the threshold voltage.[32]

In the triode region ($V_{DS} \leq V_{GS} - V_T$) there is already current flowing in the sensor and the variation in V_{DS} contributes to the magnitude of the current generated. In the saturation region, the drain current is now relatively independent of the drain-source voltage variation and is controlled only by the gate voltage. This means that at values of V_{DS} greater than saturation, the current does not vary and it is possible to clearly distinguish the difference between the currents generated by each potential applied to the gate alone.[4]

When we look at the behavior of the slopes for each value of V_{GS} and V_{DS}, we see that at V_{GS} 3 V we have the lowest slope value (red bars) and also the lowest error in the measurements for any value of V_{DS} (Figure 3). This is not the case with the following V_{GS} (from 4 to 10), where there is a variation in the slope values as the V_{GS} increases and at V_{DS} between 5, 6 and 7 V. The increased error bars for higher values of V_{DS} were also evident in Figure 3.

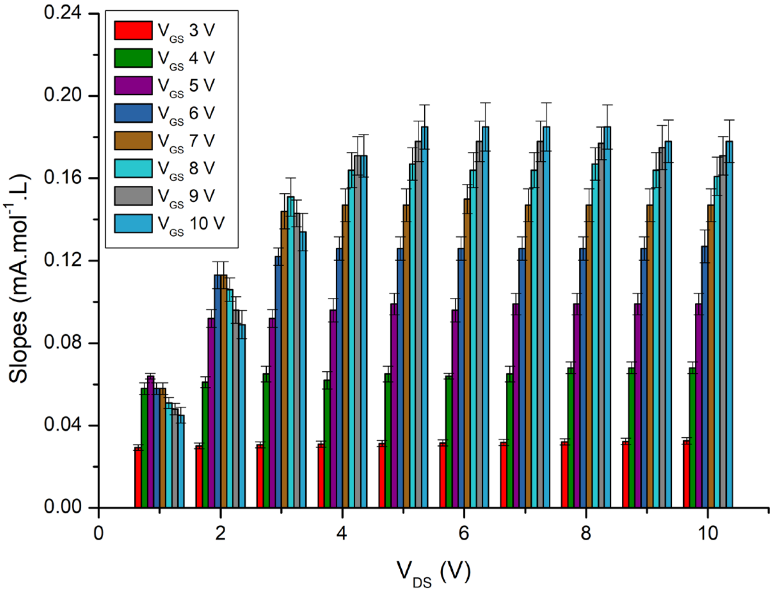

Figure 3. Slopes of measurements in chloride prepared in water using 5.5 mL of sample (1 in a static test with variable voltages between 2 and 10 V applied to the gate terminal, drain and source terminals using a Keithley Parameter Analyzer.

In addition to the slope and error values, when choosing the V_{GS} and V_{DS} values we considered the potential to V_{GS} and V_{DS} that would satisfy the MOSFET equation for the MOS saturation region ($V_{DS} \geq V_{GS} - V_T$), where the drain/source voltage is greater than the gate/source voltage and the device's turn-on voltage. In addition, we also consider the values of voltage that would increase the useful life of the transistor. The best values for this would be V_{GS} 3 and V_{DS} 5 V. So, we decided to carry out the measurements at V_{GS} 3.5 V and V_{DS} 5 V. Given these results, we were able to assign a standard V_{GS} and V_{DS} value for all the measurements.

The action of the indicator electrode is the same as that often discussed in the literature for Ag/AgCl electrodes but with the EGFETs, the indicator electrode in direct contact with the solution contributes to the formation of a double layer at the solution interface, so that the interaction of charges at the FET gate causes changes in the conductivity of the device's source-drain channel.[50,51] The characteristic I_{DS}-V_{DS} curves measured at various chloride concentrations in water, with the V_{GS} set at 3.5 V, are shown in Figure 4.

From Figures 4a and 4b, it is clear that in the saturation region (V_{DS} 1-6 V), the concentration of chloride modulates the magnitude of the source-drain current. This is because a change in the concentration of the solution alters the equilibrium state between the metal and the oxide in the FET, which results in a change in the electrical properties and in the surface potential.[49,52]

In Figures 4c and 4d, the slope of the linear curve at a V_{GS} of 3.5 V and V_{DS} of 5 V was used to obtain the sensitivity in drain-source current. Regardless of whether the measurement was static or in flow, we observed that the higher the concentration of chloride, smaller was the I_{DS}. Under these conditions, I_{DS} increases with increasing gate voltage, indicating that the EGFET exhibited excellent gate control performance.[48,51,53,54] The response sensitivity in static condition was 0.0266 $mA^{0.5}$ mol^{-1} L, while in flow condition it was 0.0234 $mA^{0.5}$ mol^{-1} L. The linearities (R^2) were 0.9952 and 0.9423 respectively with a linear range of 1.0 mol L^{-1} to 1.0x10^{-3} mol L^{-1} for the static test and from 1.0 mol L^{-1} to 1.0x10^{-4} mol L^{-1} for the flow setup.

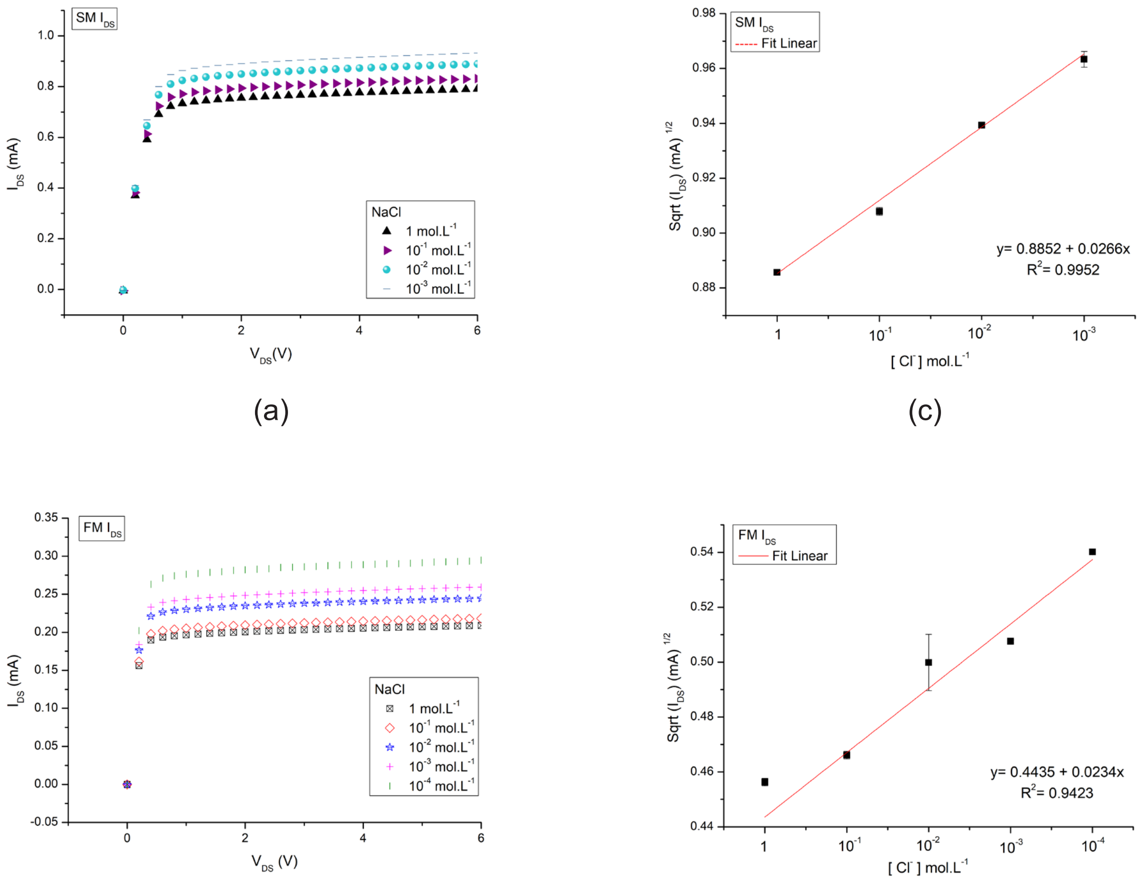

(a) (c)

(b) (d)

Figure 4. I_{DS}-V_{DS} curves at different concentrations of chloride solutions in water under static (a) and flow (b) conditions. Average I_{DS} obtained at V_{GS} 3.0 V and V_{DS} 5.0 V for different chloride concentrations static (c) and flow (d) conditions.

Transfer characteristic curves (I_{DS}-V_{GS}) are generally used to investigate the response of EGFET to analytes.[51, 55] They are carried out since the threshold voltage (V_T) cannot be measured directly, but is derived from the measurement of other parameters such as V_{GS}. V_T is used to control the on-off state of the FETs but can also be used to establish a calibration of the sensor. The characteristic I_{DS}-V_{GS} curves measured at various chloride concentrations are shown in Figure 5.

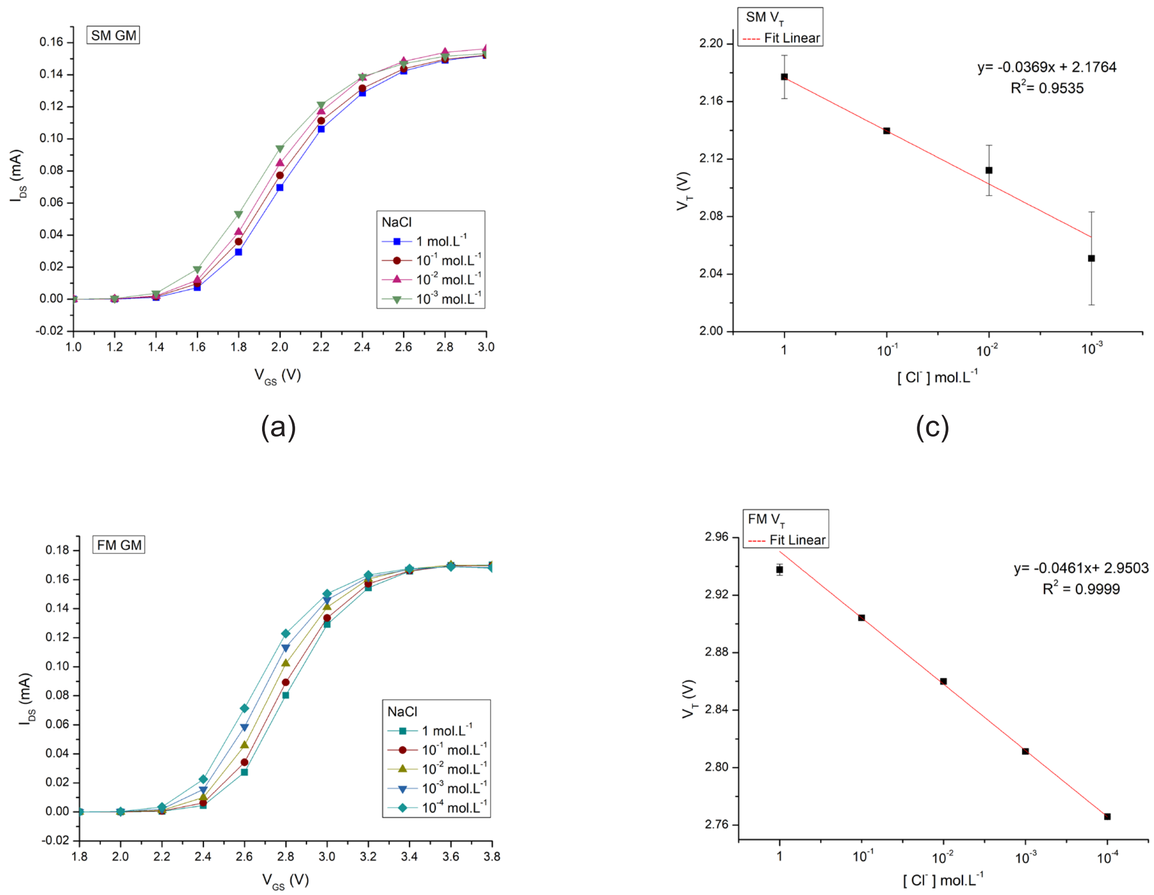

(a) (c)

(b) (d)

Figure 5. I_{DS}-V_{GS} curves for different chloride concentrations in water. Transconductance in (a) static (SM) and (b) flow (FM) modes. Threshold Voltage (VT) calibration plots in the (c) static (SM) and (d) flow (FM) modes.

The curves in Figures 5a and 5b decrease with increasing concentrations (1-10^{-4} mol L^{-1}), showing a lower V_{GS} as the concentration of the solution decreases. This shift in the curve is explained by the binding of negatively charged chloride on the surface of the extended gate. This results in a potential change on the surface of the extended gate and therefore causes a variation in the overall threshold voltage,[50] resulting in a decrease of the conductivity of the FET channel and, consequently, a a variation in I_{DS}.[56] Figures 5a and 5b show that as the concentration of the analyte decreases, the change in transconductance to a more positive value causes a gradual change in the I_{DS}-V_{GS} curves. Threshold voltage sensitivity can be obtained by observing the change in gate opening voltage as the chloride concentration decreases.

Figures 5c and 5d show that the high concentration of chloride in the solution means that more ions can be adsorbed on the EGFET gate. For the experiments discussed in these figures, we achieved a linear range of 1.0 mol L^{-1} to 1.0x10^{-3} mol L^{-1} for the static measurements and 1.0 mol L^{-1} to 1.0x10^{-4} mol L^{-1} for the flow measurements. The voltage sensitivities were 36.91 mV dec^{-1} and 46.11 mV dec^{-1} for static and flow measurement with R^2 0.9535 and 0.9999, respectively.

By decreasing the concentration of the solution there will be a point at which the response will be permanent, regardless of the concentration, or what we call an inversion can occur, which is due to the more effective positive charges on the surface, causing the voltage to behave in the opposite way to that shown in the graph in Figures 5c and 5d.[57] Table I summarizes the results for all the measures in the different matrices.

Table I. Comparison of the different current and voltage responses obtained for the samples

Sample medium and type of measurement		Sensitivity in current ($mA^{0.5}$ mol^{-1} L)	Sensitivity in voltage (mV dec^{-1})	Linearity (R^2)	LOD (mol L^{-1})	Linear range (mol L^{-1})
H_2O	SM	0.0266	36.91	0.9952 ¥ 0.9535	10^{-3}	1-10^{-3}
	FM	0.0234	46.11	0.9423 ¥ 0.9999	10^{-4}	1-10^{-4}
$NaNO_3$	SM	0.0250	52.96	0.9908 ¥ 0.9998	10^{-5} ¥10^{-3}	1-10^{-5} 1-10^{-3}
	FM	0.0181	29.87	0.8742 ¥ 0.7074	10^{-2}	1-10^{-2}
Urine	SM	0.0048	15.58	0.7855 ¥ 0.9364	10^{-3} ¥10^{-2}	1-10^{-3} 1-10^{-2}
	FM	0.0330	7.13	0.8247 ¥ 0.7581	10^{-5}	1-10^{-5}
Dilute urine*	SM	0.0275	38	0.9487 ¥ 0.8895	4	1-4
	FM	0.4759	47.4	0.8611 ¥ 1.000	3 2	1-3 1-2

*The linear range for urine corresponds to number of sample dilutions, rather than concentration in mol L^{-1}.
¥ Data for sensitivity in voltage.

Our voltage sensitivity values were higher than those of other studies already described in the literature, with much greater measurement linearity for the range investigated.[58] This is due to the excellent action of the Ag/AgCl indicator electrode in interacting with the species in the solution.

The experimental results showed that the sensitivity to the I_{DS} current of the sensor for samples in water regardless of the type of measurement, the sensitivity values are comparable. In this case, the flow system is preferable, as it allows the measurement to be automated and reduces the possibility of human error.

The voltage sensitivity showed that for the water and diluted urine samples the voltage sensitivity was approximately 10 mV dec^{-1} higher than those of other studies already described in the literature.[58] Whereas, for the $NaNO_3$ matrix and urine, the sensitivity was half the value under dynamic conditions when compared to static conditions. Because of these situations it is more common in the literature to find measurements of variation in I_{DS} rather than V_T, as more consistent values are obtained.

We also carried out detection of SCN^- prepared in synthetic biological matrices in order to compare the results of the system in these types of samples and in the detection of this ion.

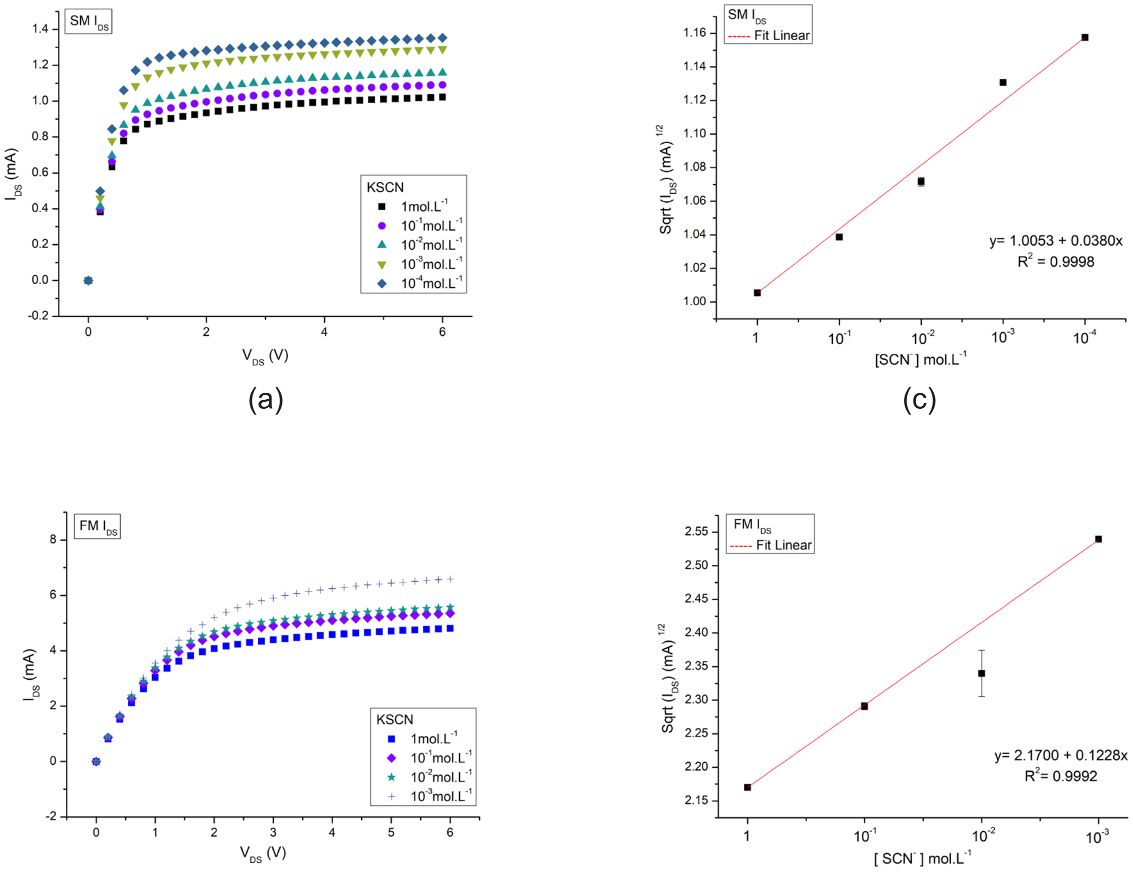

(a) (c)

(b) (d)

Figure 6. I_{DS}-V_{DS} curves for different concentrations of thiocyanate solutions in water. I_{DS}-V_{DS} curve for SM (a) and FM (b). Average current sensitivity in chloride solution prepared in water SM (c) Average sensitivity current sensitivity in the FM (d).

In Figure 6, there is a linear relationship between the I_{DS} currents for all sample concentrations. In this test, the sensitivity of the response under static conditions was 0.0380 $mA^{0.5}$ mol^{-1} L, while under dynamic conditions it was 0.1228 $mA^{0.5}$ mol^{-1} L. The linearities of the measurements were R^2 0.9998 and 0.9992, respectively, with a linear range of 1 mol L^{-1} to 10^{-4} mol L^{-1} for the static tests and 1 mol L^{-1} to 10^{-3} mol L^{-1} for the flow tests.

Transfer characteristic curves (I_{DS}-V_{GS}) were also carried out to investigate the response of EGFET to SCN^-.

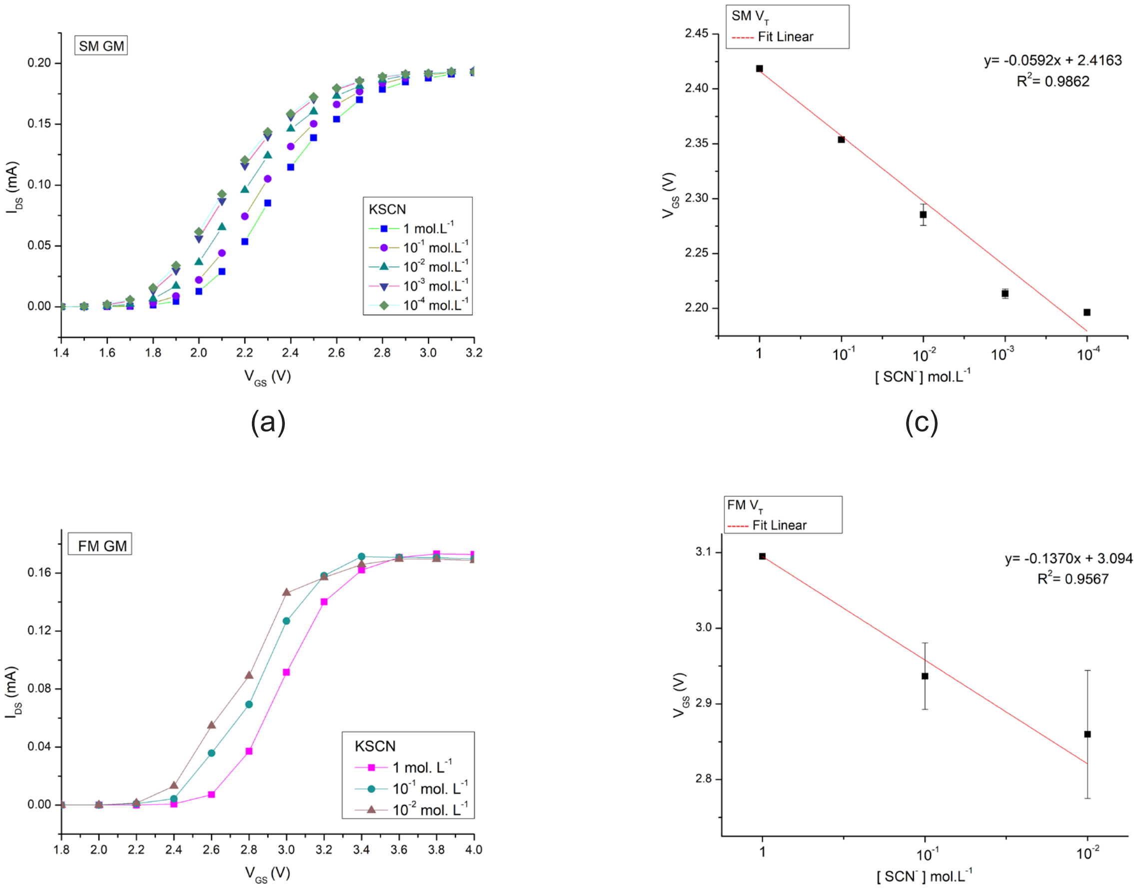

(a) (c)

(b) (d)

Figure 7. I_{DS}-V_{GS} curves for different concentrations of thiocyanate in water. Transconductance of SM tests (a) and FM (b), Current sensitivity for samples in the static test (c) and flow measurement (d).

As with the chloride tests, the curves in Figures 7a and 7b decreases as the concentrations increased (10^{-2} – 1 mol L^{-1}). As the thiocyanate ion also has a negative charge, the same situation occurs as with chloride.

For the test with these samples, we obtained a linear range of 1 mol L^{-1} to 10^{-4} mol L^{-1} for the static test, as shown in Figure 7c. And a linear range of 1 mol L^{-1} to 10^{-2} mol L^{-1} for the dynamic test, as shown in Figure 7d. The voltage sensitivity was 59.24 mV dec^{-1} for the static measurement and 137.06 mV dec^{-1} for the dynamic measurement, with R^2 0.9862 and 0.9567, respectively.

The I_{DS}-V_{GS} test showed that there are also contributions from other factors that influence the gate potential than just those related to the change in solution concentration. It is therefore important to carry out both measurement modes to eliminate possible problems. Errors can be more easily detected using current measurements (for example, poor wire connections and MOS burnout), since the data show faults like these more clearly. In the transconductance measurement, even if the Parameter Analyzer is configured to extract V_T directly, it is very important to plot a graph with the GM values obtained, observing whether any other events may be minimally influencing the sensor's final response to the measurements.

In the experiments with KSCN prepared in other matrices, the current and voltage behavior is shown in Table II.

Table II. Behavior of the different concentrations of KSCN solution prepared in DI water, saliva, sweat and urine when using 5 mL of sample in SM and 500 μL min^{-1} in FM

Sample medium and type of measurement		Sensitivity in current (mA$^{0.5}$ mol^{-1} L)	Sensitivity in voltage (mV dec^{-1})	Linearity (R^2)	LOD (mol L^{-1})	Linear range (mol L^{-1})
H_2O	SM	0.0380	59.24	0.9998 ¥ 0.9862	10^{-4}	1-10^{-4}
	FM	0.1228	137.06	0.9992 ¥ 0.9567	10^{-3} ¥10^{-2}	1-10^{-3} ¥ 1-10^{-2}
Saliva	SM	0.1762	33.14	0.8281 ¥ 0.7522	10^{-2} ¥10^{-4}	1-10^{-2} ¥ 1-10^{-4}
	FM	0.0258	83.33	0.9125 ¥ 0.8604	10^{-3}	1-10^{-3}
Sweat	SM	0.0355	33.03	0.8930 ¥ 0.9211	10^{-5} ¥10^{-3}	1-10^{-5} ¥ 1-10^{-3}
	FM	0.0345	76.20	0.7532 ¥ 0.8527	10^{-5} ¥10^{-3}	1-10^{-5} ¥ 1-10^{-3}
Urine	SM	0.0351	50.19	0.7042 ¥ 0.8759	10^{-3}	1-10^{-3}
	FM	0.0582	58.88	0.9454 ¥ 0.8481	10^{-3}	1-10^{-3}

¥ Data for sensitivity in voltage.

The sensitivity to the I_{DS} current was higher for the water and saliva samples submitted to the flow and static measurement. The voltage sensitivity was also higher in the samples submitted to flow measurements, but the linear range was decreased.[60-63]

With these measurements, we identified that the system presented, in most cases, nernstian or super-nernstian responses for values in the flow than for the static tests. The current sensitivity values obtained here are much higher than those considered in the literature, regardless of the matrix.[47]

We then went on to develop a bench measurement system (Plug Injection Analysis) that could respond linearly to variations in concentration, in which we converted the system's drain-source current measurement into voltage values using a resistor of known value and following Ohm's equation. The system designed is shown in Figure 8.

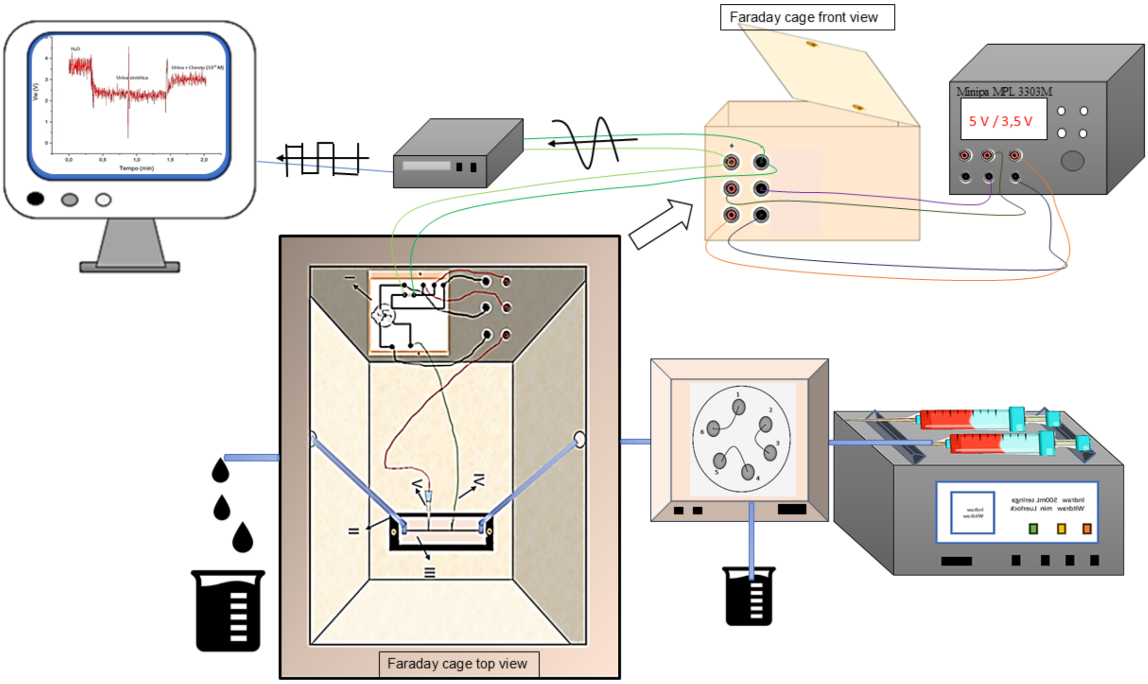

Figure 8. Measurement system for plug injection analysis.

In the system shown in Figure 8, there was a syringe pump coupled to a six-way valve that injected solvent while the flow modulator was activated to inject a small amount of sample. The electrodes were welded to a phenolite circuit board with an electrical measuring circuit (I) in which there was an 8.2 KΩ resistor at the output of the drain terminal. The sample entered the metal box used as a Faraday cage through tubes positioned on the sides of the box (II) and passed through the microfluidic chip (III) inside, passing through the indicator (IV) and control (V) electrodes. Through interconnections on the outside of the metal box, the circuit received the voltage applications and an analog-digital interface was responsible for receiving the solvent signals. When the sample was injected, the computer monitor connected to the analog-digital interface showed voltage peaks characteristic of each concentration of the solutions.

The schematics of the electrical circuit can be seen in Figure 9.

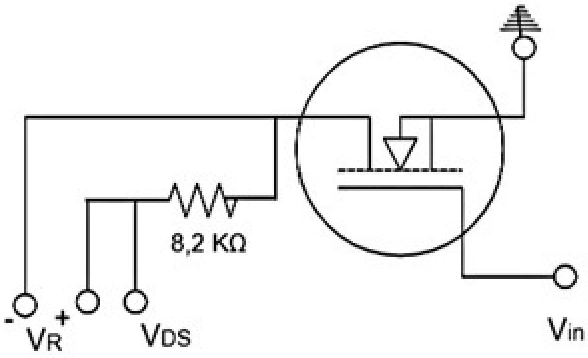

Figure 9. Electrical circuit designed for plug injection analysis.

In the circuit, the body terminal of the MOSFET was grounded to polarize it in relation to the gate of the device. There was a resistor in parallel with the drain because we were measuring the current variation in this terminal as the concentration of the solutions changed. The idea was that the resistor in parallel with the drain terminal would give us information about the output current at this terminal. Once we had obtained the current, given Ohm's equation, we calculated the voltage using Labview software with an appropriately adapted interface for this measurement. The current circulating was consequently linked to the induction of the charges on the MOSFET gate, which is why we could make this approximation.[51,64]

The probe used was connected to an analog-digital interface connected to the computer program and so it was possible to detect the increments, restricting them only to those with values above 5 V, which was the measurement limit of the analog-digital interface. In the case of plug injection analysis, each chloride concentration in the sample was responsible for a response pulse in the LabView system, since aliquots of the solution were injected every minute. Thus, higher concentrations were responsible for longer pulses.

The procedure using the system in Figure 8 was similar to that of measurement 2 described earlier in the methodology section, but the syringe pump uninterruptedly injected the blank (matrix in which the solutions were prepared). While, different concentrations of the analyte were injected by the flow modulator at certain time intervals. The I_{DS} current can be obtained by converting the voltage drop in the resistor using Ohm's law.[51] The results measured at various chloride concentrations in the plug injection analysis are shown in Figure 10.

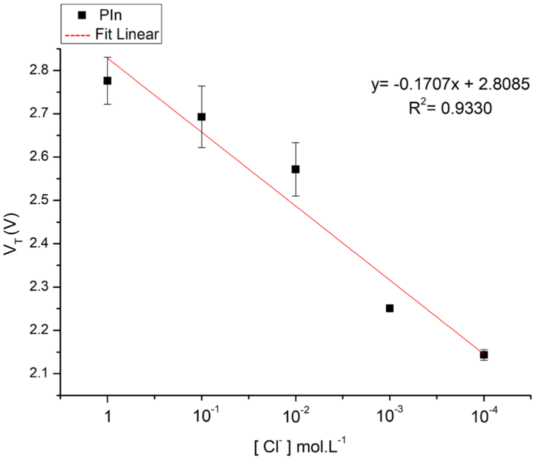

Figure 10. Potential sensitivity for samples chloride in water in the PIn setup.

For these measurements, the voltage sensitivity was 170.78 mV dec^{-1} over a wide range from 1 mol L^{-1} to 10^{-4} mol L^{-1}, with R^2 0.9330 for the samples in water. For the samples prepared in $NaNO_3$ 0.5 mol L^{-1} and urine, we obtained the data shown in Table III.

Table III. Result to measurement in plug injection analysis to chloride in different matrices

Sample	Sensitivity in voltage (mV dec^{-1})	Linearity (R^2)	LOD (mol L^{-1})	Linear range (mol L^{-1})
H_2O	170.78	0.9330	10^{-4}	$1\text{-}10^{-4}$
$NaNO_3$	83.49	0.8720	10^{-3}	$1\text{-}10^{-3}$
Urine	105	0.9436	10^{-3}	$1\text{-}10^{-3}$

The voltage sensitivity data obtained with the plug injection system cannot be directly compared with the previous values in order to confirm the success of the system, since there are differences in the resistor values used in the parameter analyzer and in the elaborate configuration. However, the success of the system can be seen in the good linearity of the response, which is considered to be above R^2 0.87 for all measurements. In addition, the linear range described in Table III shows values equivalent to the other detection ranges in the previous tables for the same solvent and analyte.

Considering that this system can receive more contributions from noise, leakage of applied potential and so on, the values obtained using it are still in a very acceptable range for it to be considered functional. For future use, we intend to optimize it by replacing the power supply with a battery system, in order to reduce the noise from electronic systems.

CONCLUSIONS

In conclusion, we have successfully fabricated chloride and thiocyanate measurement systems using EGFETs in two conventional static and dynamic measurement configurations and presented a new plug measurement configuration based on a simple system that can be adapted to be portable. With the systems used, we were able to recognize ions in different artificial biological and non-biological matrices, achieving linearity of up to R^2 0.9999 in some cases, with a detection range of at least 10^{-5} mol L^{-1}. And in the tests, chloride detection showed the greatest expansion of the linear measurement range, although in the tests with thiocyanate the variations in sensitivity given by the different concentrations of the solutions had higher results than for chloride.

As mentioned in the aim of this study, we present an in-depth discussion of EGFET's behavior in detecting ions. Based on different literature in the field, we discuss the main concepts involved in the operation of this type of sensor and how the data derived from them is usually presented graphically for the better understanding of the reader who is just starting to study EGFETs.

The systems designed showed an excellent signal-to-noise ratio, except for the plug injection measurement, which requires adaptations to reduce noise interference from electrical sources. Optimization of this battery-powered measurement system will therefore be the subject of future studies. Further optimizations in the measurement configuration for future use could also lead to better LOD values for the measurements. One of the limitations of using the flow test system developed in our study is the need for a sample volume of at least 2 mL to fill the entire flow structure and the test run time.

The device, in its current form, with a metal indicator electrode is sensitive to the ions tested, but is not selective. The development of a detection membrane selective only to chloride ions and another only to thiocyanate ions is necessary. The focus of our study so far, however, is more geared towards demonstrating the potential of EGFET-based configurations for the determination of various analytes.

We hope that this study will contribute to the scientific community's understanding of new field-effect sensor systems, an area that has expanded significantly in recent years.

Conflicts of interest

The authors declare no conflict of interest.

Acknowledgements

This research was funded by "Fundação de Amparo à Pesquisa do Estado de São Paulo" (FAPESP) grant numbers 2018/06478-3 and 2014/50867-3, "Coordenação de Aperfeiçoamento de Pessoal do Ensino Superior" (CAPES) as scholarships and "Conselho Nacional de Desenvolvimento Científico e Tecnológico" (CNPq) grant number 465389/2014-7.

REFERENCES

(1) Mello, H. J. N. P. D.; Bueno, P. R.; Mulato, M. Comparing glucose and urea enzymatic electrochemical and optical biosensors based on polyaniline thin films. *Anal. Methods* **2020**, *12* (34), 4199–4210. http://dx.doi.org/10.1039/D0AY01018A

(2) Chiang, J.-L.; Shang, Y.-G.; Yadlapalli, B. K.; YU, F.-P.; Wuu, D.-S. Ga_2O_3 nanorod-based extended-gate field-effect transistors for pH sensing. *Materials Science and Engineering: B* **2022**, 276. https://doi.org/10.1016/j.mseb.2021.115542

(3) Oliveira, D. C. B.; Costa, F. H. M.; Silva, J. A. F. The Integration of Field Effect Transistors to Microfluidic Devices. *Micromachines* **2023**, *14* (4). https://doi.org/10.3390/mi14040791

(4) Pan, T. M.; Hsiung, H. M.; Chen, C. H.; Her, J. L. Fast and label-free detection of procalcitonin in human serum for sepsis using a WTex-based extended-gate field-effect transistor biossensor. *Biosens. Bioelectron.* **2025**, *268*. https://doi.org/10.1016/j.bios.2024.116894

(5) Bhattacharyya, I. M.; Cohen, S.; Shalabny, A.; Bashouti, M.; Oliveira, B.; Shalev, G. Specific and label-free immunosensing of protein-protein interactions with silicon-based immunoFETs. *Biosens. Bioelectron.* **2019**, *132*, 143-161. https://doi.org/10.1016/j.bios.2019.03.003

(6) Smith, K.C. *Microelectronics circuits*, 6th ed.; Oxford University Press: Oxford, New York, 2011.

(7) Pullano, S. A.; Critello, C. D.; Mahbub, I.; Tasneem N. T.; Shamsir, S.; Islam, S. K.; Greco, M.; Fiorillo, A. S. Egfet-based sensors for bioanalytical applications: A review. *Sensors* **2018**, *18* (11). https://www.mdpi.com/1424-8220/18/11/4042

(8) Koklu, A.; Ohayon, D.; Wustoni, S.; Hama, A.; Chen, X.; McCulloch, I.; Inal, S. Microfluidics integrated n-type organic electrochemical transistor for metabolite sensing. *Sens. Actuators, B* **2021**, *329*. https://doi.org/10.1016/j.snb.2020.129251

(9) Sedra, A. S.; Smith, K. C. *Microelectronic Circuits*, 5th ed. Oxford University Press, 2004.

(10) Seidel, K. F.; Koehler, M. Modified Lampert triangle in an organic field effect transistor with traps. *Phys. Rev.* **2008**, *78*. https://doi.org/10.1103/PhysRevB.78.235308

(11) Lilienfeld, J. E. *Amplifier for electric currents*. EUA, **1928**, 324, 794. https://patents.google.com/patent/US1877140A/en

(12) Cava, C. E.; Possagno, R.; Schnitzler, M. C.; Roman, P. C.; Oliveira, M. M.; Lepiensky, C. M.; Zarbin, A. J. G.; Roman, L. S. Iron- and iron oxide-filled multi-walled carbon nanotubes: Electrical properties and memory devices. *Chem. Phys. Lett.* **2007**, *444* (4-6), 304-308. https://doi.org/10.1016/j.cplett.2007.07.029

(13) Seidel, K. F.; Rossi, L.; Mello, R. M. Q.; Hummelgen, I. A. Vertical organic field effect transistor using sulfonated polyaniline/aluminum bilayer as intermediate electrode. *J. Mater. Sci.:Mater. Electron.* **2013**, *24*, 1052-1056. https://doi.org/10.1007/s10854-012-0876-5

(14) Skoog, D.; West, D.; Holler, J.; Crouch, S. *Fundamentals of Analytical Chemistry*. Cengage Learning, 2014.

(15) Tiwari, N.; Chatterjee, S.; Kaswan, K.; Chung, J.-H.; Fan, K.-P.; Lin, Z.-H. Recent advancements in sampling, power management strategies and development in applications for non-invasive wearable electrochemical sensors. *J. Electroanal. Chem.* **2022**, *907*. https://doi.org/10.1016/j.jelechem.2022.116064

(16) Sinha, A.; Tai, T. Y.; Li, K. H.; Gopinathan, P.; Chung, Y. D.; Sarangadharan, I.; Ma, H. P.; Huang, P. C.; Shiesh, S. C.; Wang, Y. L.; et al. An integrated microfluidic system with field-effect-transistor sensor arrays for detecting multiple cardiovascular biomarkers from clinical samples. *Biosens. Bioelectron*. **2019**, *129*, 155-163. https://doi.org/10.1016/j.bios.2019.01.001

(17) Cheng, Y.; Chen, K. S.; Meyer, N. L.; Yuan, J.; Hirst, L. S.; Chase, P. B.; Xiong, P. Functionalized SnO_2 nanobelt field-effect transistor sensors for label-free detection of cardiac troponin. *Biosens. Bioelectron.* **2011**, *26* (11), 4538-4544. https://doi.org/10.1016/j.bios.2011.05.019

(18) Chou, C.-H.; Lim, J.-C.; Lai, Y.-H.; Chen, Y.-T.; Lo, Y.-H.; Huang, J.-J. Characterizations of protein-ligand reaction kinetics by transistor-microfluidic integrated sensors. *Anal. Chim. Acta* **2020**, *1110*, 1-10. https://doi.org/10.1016/j.aca.2020.03.012

(19) Chen, T.-Y.; Yang, T.-H.; Wu, N.-T.; Chen, Y.-T.; Huang, J.-J. Transient analysis of streptavidin-biotin complex detection using an igzo thin film transistor-based biosensor integrated with a microfluidic channel. *Sens. Actuators, B* **2017**, *244*, 642-648. https://doi.org/10.1016/j.snb.2017.01.050

(20) Khizir, H. A.; Abbas, T. A.-H. Hydrothermal synthesis of TiO_2 nanorods as sensing membrane for extended-gate field-effect transistor (egfet) pH sensing applications. *Sens. Actuators, A* **2022**, *333*. https://doi.org/10.1016/j.sna.2021.113231

(21) Manjakkal, L.; Sakthivel, B.; Gopalakrishnan, N.; Dahiya, R. Printed flexible electrochemical pH sensors based on cuo nanorods. *Sens. Actuators, B* **2018**, *263*. https://doi.org/10.1016/j.snb.2018.02.092

(22) Casimero, C.; McConville, A.; Fearon, J.-J.; Lawrence, C. L.; Taylor, C. M.; Smith, R. B.; Davis, J. Sensor systems for bacterial reactors: A new flavin-phenol composite film for the in situ voltammetric measurement of pH. *Anal. Chim. Acta* **2018,** *1027*, 1-8. https://doi.org/10.1016/j.aca.2018.04.053

(23) Cho, W.-J.; Lim, C.-M. Sensing properties of separative paper-based extended-gate ion-sensitive field-effect transistor for cost effective pH sensor applications. *Solid-State Electron.* **2017**, *140*, 96-99. https://doi.org/10.1016/j.sse.2017.10.025

(24) Rasheed, H. S.; Ahmed, N. M.; Matjafri, M. Ag metal mid layer based on new sensing multilayers structure extended gate field effect transistor (EG-FET) for pH sensor. *Mater. Sci. Semicond. Process.* **2018**, *74*, 51-56. https://doi.org/10.1016/j.mssp.2017.10.011

(25) Slewa, L. H.; Abbas, T. A.; Ahmed, N. M. Synthesis of quantum dot porous silicon as extended gate field effect transistor (EGFET) for a pH sensor application. *Mater. Sci. Semicond. Process.* **2019**, *100*, 167-174. https://doi.org/10.1016/j.mssp.2019.04.045

(26) Kang, J.-W.; Cho, W.-J. Achieving enhanced pH sensitivity using capacitive coupling in extended gate fet sensors with various high-k sensing films. *Solid-State Electron.* **2019**, *152*, 29-32. https://doi.org/10.1016/j.sse.2018.11.008

(27) Bazilah, A.; Awang, Z.; Sobihana, S. S.; Hazirah, N. H.; Herman, S. H. Sensing and physical properties of ZnO nanostructures membrane. *Mater. Today: Proc.* **2019**, *16* (4), 1864-1870. https://doi.org/10.1016/j.matpr.2019.06.062

(28) Rocha, D. L.; Rocha, F. R. P. An environmentally friendly flow-based procedure with photoinduced oxidation for the spectrophotometric determination of chloride in urine and waters. *Microchem. J.* **2013**, *108*, 193-197. https://doi.org/10.1016/j.microc.2012.10.020

(29) Farrell, P. M.; Rosenstein, B. J.; White, T. B.; Accurso, F. J.; Castellani, C.; Cutting, G. R.; Durie, P. R.; Legrys, V. A.; Massie, J.; Parad, R. B.; Rock, M. J. Campbell, P. W. Guidelines for diagnosis of cystic fibrosis in newborns through older adults: Cystic Fibrosis Foundation consensus report. *J. Pediatr.* **2008,** *153* (2), PS4-S14. https://doi.org/10.1016/j.jpeds.2008.05.005

(30) Lien, Y-H. H. Urine Tests for Chronic Hypokalemia: When in Doubt, Check Urine-Sodium-to-Chloride Ratio. *Am. J. Med.* **2017**, *130* (7), 761-762. https://doi.org/10.1016/j.amjmed.2017.02.040

(31) Zhang, W.; Huang, S.; Zhang, Y.; Lv, H.; Ge, D.; Gu, Y.; Jiang, M. Cesium lead bromide perovskite nanocrystals for the visual detection of chloride ions: A review. *J. Solid State Chem.* **2024**, *329*. https://doi.org/10.1016/j.jssc.2023.124418

(32) Cui, X.; Wei, T.; Hao, M.; Qi, Q.; Wang, H.; Dai, Z. Highly sensitive and selective colorimetric sensor for thiocyanate based on electrochemical oxidation-assisted complexation reaction with Gold nanostars etching. *J. Hazard. Mater.* **2020**, *391*. https://doi.org/10.1016/j.jhazmat.2020.122217

(33) Nemakal, M.; Giddaerappa, S.; Palanna, M.; Sannegowda, L. K.; Kumar, P. S. Zinc phthalocyanine anchored magnetite particles: Efficient platform for sensing of thiocyanate. *J. Electroanal. Chem.* **2021**, *895*. https://doi.org/10.1016/j.jelechem.2021.115385

(34) Guan, J.; Wan, Y.; Li, J.; Zheng, T.; Xia, W.; Xu, S.; Li, Y. Urinary perchlorate, thiocyanate, and nitrate and their associated risk factors among Chinese pregnant women. *Chemosphere* **2023**, *345*. https://doi.org/10.1016/j.chemosphere.2023.140467

(35) Wang, Z.; Ma, C.; Wu, Y.; Gu, J.; Zhu, C.; Li, L.; Gao, H.; Yang, Z.; Li, X.; Wei, Y.; Wang, G.; Guo, S.; Chen, G. A sensitive method for detecting sodium thiocyanate using AgNPs and MIL-101(Fe) combined as SERS substrate. *Vib. Spectrosc.* **2021**, *117*. https://doi.org/10.1016/j.vibspec.2021.103311

(36) Rajendran, J. Amperometric determination of salivary thiocyanate using electrochemically fabricated poly (3,4-ethylenedioxythiophene)/MXene hybrid film. *J. Hazard. Mater.* **2023**, *449*. https://doi.org/10.1016/j.jhazmat.2023.130979

(37) Shirmardi, A.; Shamsipur, M.; Akhond, M.; Monjezi, J. Electronic tongue for simultaneous determination of cyanide, thiocyanate and iodide. *Measurement* **2016**, *88*, 27-33. https://doi.org/10.1016/j.measurement.2016.03.038

(38) Wirojsaengthong, S.; Aryuwananon, D.; Aeungmaitrepirom, W.; Pulpoka, B.; Tuntulani, T. A colorimetric paper-based optode sensor for highly sensitive and selective determination of thiocyanate in urine sample using cobalt porphyrin derivative. *Talanta* **2021**, *231*. https://doi.org/10.1016/j.talanta.2021.122371

(39) Silva, M.; Sako, A. V. F.; Micke, G. A.; Vitali, L. A rapid method for simultaneous determination of nitrate, nitrite and thiocyanate in milk by CZE-UV using quaternary ammonium chitosan as electroosmotic flow inverter. *J. Food Compos. Anal.* **2020**, *88*. https://doi.org/10.1016/j.jfca.2020.103455.

(40) Afkhami, A.; Soltani-Felehgari, F.; Madrakian, T. Highly sensitive and selective determination of thiocyanate using gold nanoparticles surface decorated multi-walled carbon nanotubes modified carbon paste electrode. *Sens. Actuators, B* **2014**, *196*, 467-474. https://doi.org/10.1016/j.snb.2014.01.115

(41) Pholsiri, T.; Khamcharoen, W.; Vimolmangkang, S.; Siangproh, W.; Chailapakul, O. Paper-based electrochemical sensor for simultaneous detection of salivary Δ^9-tetrahydrocannabinol and thiocyanate to differentiate illegal cannabis smokers. *Sens. Actuators, B* **2023**, *383*. https://doi.org/10.1016/j.snb.2023.133571

(42) Urbanowicz, M.; Sadowska, K.; Pijanowska, D. G.; Pomećko, R.; Bocheńska, M. Potentiometric Solid-Contact Ion-Selective Electrode for Determination of Thiocyanate in Human Saliva. *Sensors* **2020**, *20* (10). https://doi.org/10.3390/s20102817

(43) Saravanan, S.; Rani, T. M. S.; Nazare, A. D.; Nutalapati, V.; Maji, S. Fluorometric detection of fluoride and thiocyanate ions using novel anthrapyrazolone derivatives. *Mater. Today: Proc.* **2021**, *40* (S1), S241-S247. https://doi.org/10.1016/j.matpr.2020.11.149

(44) Singh, K.; Lou, B-S.; Her, J-L.; Pang, S-T.; Pan, T-M. Super Nernstian pH response and enzyme-free detection of glucose using sol-gel derived RuOx on PET flexible-based extended-gate field-effect transistor. *Sens. Actuators, B* **2019**, *298*. https://doi.org/10.1016/j.snb.2019.126837

(45) Wang, C-W.; Pan, T-M. Structural properties and sensing performances of CoN_xO_y ceramic films for EGFET pH sensors. *Ceram. Int.* **2021**, *47* (18), 25440-25448. https://doi.org/10.1016/j.ceramint.2021.05.266

(46) Chang, S-P.; Yang, T-H. Sensing Performance of EGFET pH Sensors with CuO Nanowires Fabricated on Glass Substrate. *Int. J. Electrochem. Sci.* **2012**, *7* (6), 5020-5027. https://doi.org/10.1016/S1452-3981(23)19600-3

(47) Majd, S. M.; Salimi, A. Microfluidic electrolyte-gated TiS_3 nanoribbons-based field-effect transistor as ultrasensitive label-free immunosensor for prostate cancer marker analysis. *Sensing and Bio-Sensing Research* **2024**, *43*. https://doi.org/10.1016/j.sbsr.2024.100627

(48) Al-Diabat, A. M.; Algadri, N. A.; Alzoubi, T.; Ahmed, N. M.; Noqta, O. A.; Makhadmeh, G. N.; Abuelsamen, A.; Abdelgalil, A.; Ali, A. M. A. Synthesis of Al quantum dots on porous silicon as an effective radiation detector using extended gate technique. *Results Eng.* **2024**, *21*. https://doi.org/10.1016/j.rineng.2024.101973

(49) Al-Qahtani, H. R.; Al-Odayni, A-B. M.; Zeama, M.; Shekhah, O.; Eddaoudi, M.; Grell, M. Metal-organic frameworks as sensitisers for potentiometric sensors. *Microchem. J.* **2024**, *201*. https://doi.org/10.1016/j.microc.2024.110547

(50) Hatada, M.; Pavlidis, S.; Sode, K. Development of a glycated albumin sensor employing dual aptamer-based extended gate field effect transistors. *Biosens. Bioelectron.* **2024**, *251*. https://doi.org/10.1016/j.bios.2024.116118

(51) Pan, T-M.; Lin, L-A.; Ding, H-Y.; Her, J-L.; Pang, S-T. A simple and highly sensitive flexible sensor with extended-gate field-effect transistor for epinephrine detection utilizing InZnSnO sensing films. *Talanta* **2024**, *275*. https://doi.org/10.1016/j.talanta.2024.126178

(52) Yadlapalli, B. K.; Chou, H-Y.; Chiang, J-L.; Wuu, D-S. Morphological investigation and pH sensing properties of β-Ga_2O_3 EGFET-pH sensor. *Materials Science and Engineering: B* **2024**, *300*. https://doi.org/10.1016/j.mseb.2023.117113

(53) Al-Diabat, A. M.; Algadri, N. A.; AlZoubi, T.; Ahmed, N. M.; Noqta, O. A.; Makhadmeh, G. N.; Abuelsamen, A.; Ali, A. M. A. Advancement in embedding Pb quantum dots into a Porous-Si matrix for superior X-ray radiation detection: An extended gate approach. *Radiat. Meas.* **2024**, *176*. https://doi.org/10.1016/j.radmeas.2024.107183

(54) Yu, S.; Pan, Y.; Tang, L.; Wu, S.; Liang, C.; Zhang, G-J.; Li, Y-T. Integrated Microfluidic-Transistor Sensing System for Multiplexed Detection of Traumatic Brain Injury Biomarkers. *ACS Sens.* **2024**, *9* (6), 3017-3026. https://doi.org/10.1021/acssensors.4c00194

(55) Siebel, O. F.; Schneider, M. C.; Galup-Montoro, C. MOSFET threshold voltage: Definition, extraction, and some applications. *Microelectron. J.* **2012**, *43* (5), 329-336. https://doi.org/10.1016/j.mejo.2012.01.004

(56) Pan, T-M.; Shih, C-Y.; Lin, L-A. Engineering Ta-doped $MoSe_x$ sensitive films in extended-gate field-effect transistors for ultrahigh sensitivity detection of epinephrine at fM levels. *J. Ind. Eng. Chem.* **2024**, *142*, 348-358. https://doi.org/10.1016/j.jiec.2024.07.040

(57) Yang, C-M.; Wei, C-H.; Ughi, F.; Chang, J-Y.; Pijanowska, D. G.; Lai, C-S. High pH stability and detection of α-synuclein using an EGFET biosensor with an HfO_2 gate deposited by high-power pulsed magnetron sputtering. *Sens. Actuators, B* **2024**, *416*. https://doi.org/10.1016/j.snb.2024.136006

(58) Chou, J.-C.; Ye, G.-C.; Wu, D.-G.; Chen, C.-C. Fabrication of the array chlorine ion sensor based on microfluidic device framework. *Solid-State Electron.* **2012**, *77*, 87-92. https://doi.org/10.1016/j.sse.2012.05.021

(59) Tseng, S. C.; Wu, T. Y.; Chou, J. C.; Liao, Y. H.; Lai, C. H.; Chen, J. S.; Yan, S. J.; Huang, M. S.; Tseng, T. W.; Nien, Y. H. Research of sensing characteristic and dynamic measurement of graphene oxides modified flexible arrayed RuO_2 chlorine ion sensor. *Mater. Res. Bull*. **2018**, *101*, 155-161. https://doi.org/10.1016/j.materresbull.2018.01.015

(60) Kim, D. S.; Park, J. E.; Shin, J. K.; Kim, P. K.; Lim, G.; Shoji, S. An extended gate FET-based biosensor integrated with a Si microfluidic channel for detection of protein complexes. *Sens. Actuators, B* **2006**, *117* (2), 488-494. https://doi.org/10.1016/j.snb.2006.01.018

(61) Adam, H.; Gopinath, S. C. B.; Arshad, M. K. M.; Adam, T.; Hashim, U.; Sauli, Z.; Fakhri, M. A.; Subramaniam, S.; Chen, Y.; Sasidharan, S.; Wu, Y. S. Integration of microfluidic channel on electrochemical-based nanobiosensors for monoplex and multiplex analyses: An overview. *J. Taiwan Inst. Chem. Eng.* **2023**, *146*. https://doi.org/10.1016/j.jtice.2023.104814

(62) Roman, G. T.; Kennedy, R. T. Fully integrated microfluidic separations systems for biochemical analysis. *J. Chromatogr. A* **2007**, *1168* (1-2), 170-188. https://doi.org/10.1016/j.chroma.2007.06.010

(63) Ghafouri, T.; Manavizadeh, N. A 3D-printed millifluidic device for triboelectricity-driven pH sensing based on ZnO nanosheets with super-Nernstian response. *Anal. Chim. Acta* **2023**, *1267*. https://doi.org/10.1016/j.aca.2023.341342

(64) Cao, S.; Sun, P.; Xiao, G.; Tang, Q.; Sun, X.; Zhao, H.; Zhao, S.; Lu, H.;Yue, Z. ISFET-based sensors for (bio)chemical applications: A review. *Electrochem. Sci. Adv.* **2023**, *3* (4). https://doi.org/10.1002/elsa.202100207